Theoretical prediction of a strongly correlated Dirac metal

I. I. Mazin,[1] Harald O. Jeschke,[2] Frank Lechermann,[3] Hunpyo Lee,[2] Mario Fink,[4] Ronny Thomale,[4] and Roser Valentí[2]

[1]*Code 6393, Naval Research Laboratory, Washington, DC 20375, USA*
[2]*Institut für Theoretische Physik, Goethe-Universität Frankfurt, Max-von-Laue-Strasse 1, 60438 Frankfurt am Main, Germany*
[3]*I. Institut für Theoretische Physik, Universität Hamburg, D-20355 Hamburg, Germany*
[4]*Institut für Theoretische Physik I, Universität Würzburg, am Hubland, 97074 Würzburg, Germany*

(Dated: March 5, 2014)

Recently, the most intensely studied objects in the electronic theory of solids have been strongly correlated systems and graphene. However, the fact that the Dirac bands in graphene are made up of sp^2-electrons, which are subject to neither strong Hubbard repulsion U nor strong Hund's rule coupling J creates certain limitations in terms of novel, interaction-induced physics that could be derived from Dirac points. Here we propose $GaCu_3(OH)_6Cl_2$ (Ga-substituted herbertsmithite) as a correlated Dirac-Kagome metal combining Dirac electrons, strong interactions and frustrated magnetism. Using density functional theory (DFT), we calculate its crystallographic and electronic properties, and observe that it has symmetry-protected Dirac points at the Fermi level. Its many-body physics is excitingly rich, with possible charge, magnetic and superconducting instabilities. Through a combination of various many-body methods we study possible symmetry-lowering phase transitions such as Mott-Hubbard, charge or magnetic ordering, and unconventional superconductivity, which in this compound assumes an f-wave symmetry.

Introduction. It is well known theoretically that graphene is not the only system where crystallography, combined with a particular one-electron Hamiltonian, creates symmetry-protected Dirac points at a certain filling. As such, the hope persists to combine features of Dirac fermions and strong correlations in an experimentally accessible condensed matter system. For instance, the single-orbital kagome tight-binding model is known to feature, besides a flat band that has been subject of considerable interest, symmetry-protected Dirac points at a filling of $n = 4/3$ electrons per site (or, equivalently, $1/3$, for reversed sign of the hopping). However, so far this fact has been considered more a numerical curiosity of a simplified model than an accessible feature in real materials, and has received little attention. Currently, the predominantly studied kagome material has been herbertsmithite[1–3], $ZnCu_3(OH)_6Cl_2$, presumed to host a spin liquid with fractionalized spin excitations, consistent with recent neutron scattering measurements[4]. It might be the first manifestation of a truly two-dimensional resonating valence bond (RVB) spin liquid anticipated in theory 27 years ago[5–8], which is supported by large-scale numerical investigations[9–11].

Herbertsmithite[12] is the starting point of our proposal to unify strong correlations, metallicity and Dirac fermions. As opposed to the flat band which only exists in the nearest neighbour single-orbital tight binding model, the Dirac points in the kagome compounds are symmetry-protected and survive in any electronic structure model that respects the hexagonal symmetry. By replacing Zn^{2+} by Ga^{3+} in herbertsmithite, $GaCu_3(OH)_6Cl_2$ (Fig. 1), the Dirac points are placed at the Fermi level. These states are formed by the strongly correlated ($U/t \sim 50$) Cu$-d_{x^2-y^2}$ orbitals, whose nearest neighbour hopping Hamiltonian on the kagome lattice appears to be equivalent to that of s-orbitals. As we will further elaborate on below, we find a strong, compared to graphene, screening, hinting at rather local interactions, while the nature of magnetic interactions is typical for the kagome lattice, suggesting no long range antiferromagnetism and a flat spin fluctuation profile.

Zn and Ga are neighbours in the periodic table and their radii are similar. Even if they do not form a continuous solid solution, our calculations suggest that the fully substituted compound, $GaCu_3(OH)_6Cl_2$, should be dynamically stable, and it should be possible to dope it with holes by partially replacing Ga with Zn. If the solid solution $Zn_{1-x}Ga_xCu_3(OH)_6Cl_2$ were to exist, it would span the whole range from a fully frustrated RVB spin liquid ($x = 0$) at half filling $n = 1$ to a strongly correlated Dirac metal ($x = 1$) at $n = 4/3$. The ground state in the former limit is known to be a uniform Mott insulator. Upon doping, a number of instabilities can manifest themselves, and in fact one can anticipate a complex and highly interesting phase diagram. Specifically, the DFT noninteracting one-electron picture may be prone to (1) Mott-Hubbard metal-insulator transition, (2) charge ordering, (3) ferromagnetism or (4) a superconducting instability. Below we will first present our DFT calculations, and then discuss these possible instabilities by means of various complementary many-body model approaches.

First principles calculations. Herbertsmithite is part of the Zn-paratacamite family of compounds[3] that shows great flexibility in its composition both naturally (*e.g.,* Ni-herbertsmithite[13]) and synthetically (*e.g.* Mg-herbertsmithite[14]). While Ga more commonly assumes a fourfold coordination, it also occurs in the sixfold one[15]. In the framework of DFT we fully relaxed the herbert-

smithite structure after replacing Zn by Ga (see the Supplementary Information).

The resulting electronic structure (Fig. 2 b) shows low-energy bands qualitatively similar to a one-orbital model on the kagome lattice (Fig. 2 a) and has Dirac points exactly at the Fermi level. In order to understand this fact, we first observe that Cu in this structure sits inside an oxygen square, so that the $d_{x^2-y^2}$ orbitals, with strong $pd\sigma$ hopping to the oxygens, form a high-lying antibonding band (Fig. 3). If one neglects the other d orbitals, and integrates out oxygens, one gets a tight-binding model, which is mathematically equivalent to a single s-orbital model with the nearest neighbour hopping $t = t_{pd\sigma}^2/(E_F - E_p) > 0$. The solution of this model is well known (Fig. 2 **a**). The bands crossing along the $\Gamma - K$ line have different parity with respect to the $y/-y$ transformation ($y \perp \Gamma K$) , and therefore the Dirac points at K are symmetry-protected for an arbitrary hopping range (apart from the very small spin-orbit coupling).

The kagome tight-binding model has Dirac points at K; however, this is not the case for a finite k_z dispersion and rhombohedral symmetry (Fig. 2 **c**). In a planar system with hexagonal symmetry one can travel from Γ to M and then continue to another Γ. In a rhombohedral structure, if one travels along the same direction one actually ends up at Z, and the $k_z = 0$ plane alone has lower symmetry than if averaged over all k_z. The Dirac points remain nevertheless protected, but form a 3D line meandering about the vertical line passing through the hexagonal K point (see Fig. S1 in the Supplementary Information), which, if averaged over k_z, projects onto this point. When doped, the Fermi surface consists of six tubes that slightly twist as we move along k_z (Fig. 2 **f**, **g**).

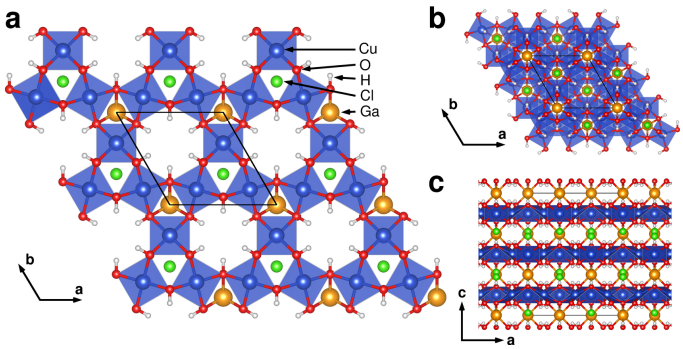

FIG. 1: Structure of predicted herbertsmithite modification $GaCu_3(OH)_6Cl_2$. **a** View of an individual kagome plane. **b** Full view along c axis where three shifted kagome layers are stacked. **c** Side view.

Normal state instabilities.- Next we want to check the system against normal state electronic instabilities. In a strongly correlated system this cannot be adequately addressed within the DFT. Therefore, we have constructed a many-body model Hamiltonian that captures the most important interactions:

$$\begin{aligned} \mathcal{H} &= \mathcal{H}_0 + \mathcal{H}_{\text{int}} \\ \mathcal{H}_0 &= \sum_{i,j}\sum_{\sigma} t_{ij} c^\dagger_{i,\sigma} c_{j,\sigma} + \mu \sum_{i,\sigma} c^\dagger_{i,\sigma} c_{i,\sigma} \\ \mathcal{H}_{\text{int}} &= U \sum_i n_{i,\uparrow} n_{i,\downarrow} + \frac{V}{2} \sum_{<i,j>} \sum_{\sigma,\sigma'} n_{i,\sigma} n_{j,\sigma'}. \end{aligned} \tag{1}$$

where the first term is the effective Cu $d_{x^2-y^2}$ tight-binding Hamiltonian derived from the DFT band structure (see the Supplementary Information) and the onsite U and nearest-neighbor Coulomb repulsion V between Cu $d_{x^2-y^2}$ atoms we estimated (see the Supplementary Information) to be $U = 5 - 7$ eV and $V = 0.11$eV. It is worth noting that the latter number is unexpectedly small. The reason for that is twofold: first, even at the exact $n = 4/3$ filling, where the metallic density of states (DOS) is zero, the behaviour of the dielectric constant is nearly metallic, and the Coulomb interaction is well screened; second, even though the electronic structure is quasi-2D, it is a far cry from an isolated plane as in graphene — each plane participates in screening interactions not only within the plane, but in all other planes.

Mott-Hubbard instability.- $ZnCu_3(OH)_6Cl_2$ is a Mott insulator since the Cu $d_{x^2-y^2}$ state is half-filled and electron hopping incurs an energy cost of U. This is not the case in $GaCu_3(OH)_6Cl_2$. Its filling of $n = 4/3$ corresponds to one electron per site plus one extra electron per three sites. Suppose $U = \infty$. Then exactly 1/3 of all sites are double, and the rest are single occupied. Thus, one electron per site will be localised and 1/3 of an electron mobile, and this mobility will not be impeded at all. This simplistic treatment suggests that the system will be metallic.

To verify that, we applied to the Hamiltonian Eq. 1 the dynamical cluster approximation (DCA) within the rotationally invariant slave-boson, DCA(RISB), formalism[16,17] in the saddle-point approximation (see the Supplementary Information). As a minimal cluster we considered three sites. Figure 4 shows our DCA(RISB) results in the paramagnetic regime. For $U = 5$ eV, we observe a band-narrowing but the essential low energy features, especially the pseudogap reflecting the Dirac points, remain. Thus, the onsite repulsion alone is insufficient to drive the system insulating at $n = 4/3$. This is a key result, and we have confirmed it by using the more accurate continuous–time quantum Monte Carlo approach (see the Supplementary Information).

Charge ordering.- Having verified the absence of a Mott-Hubbard transition, we turn to possible charge ordering, which in the limit $U \gg t$ is controlled by the intersite Coulomb repulsion V. At the mean-field level, the competition is between the energy gain of charge ordering, and the loss of kinetic energy. The former can be estimated from the fact that in the charge ordered state no neighbouring sites are doubly occupied, thus, the nearest neighbour repulsion is completely avoided.

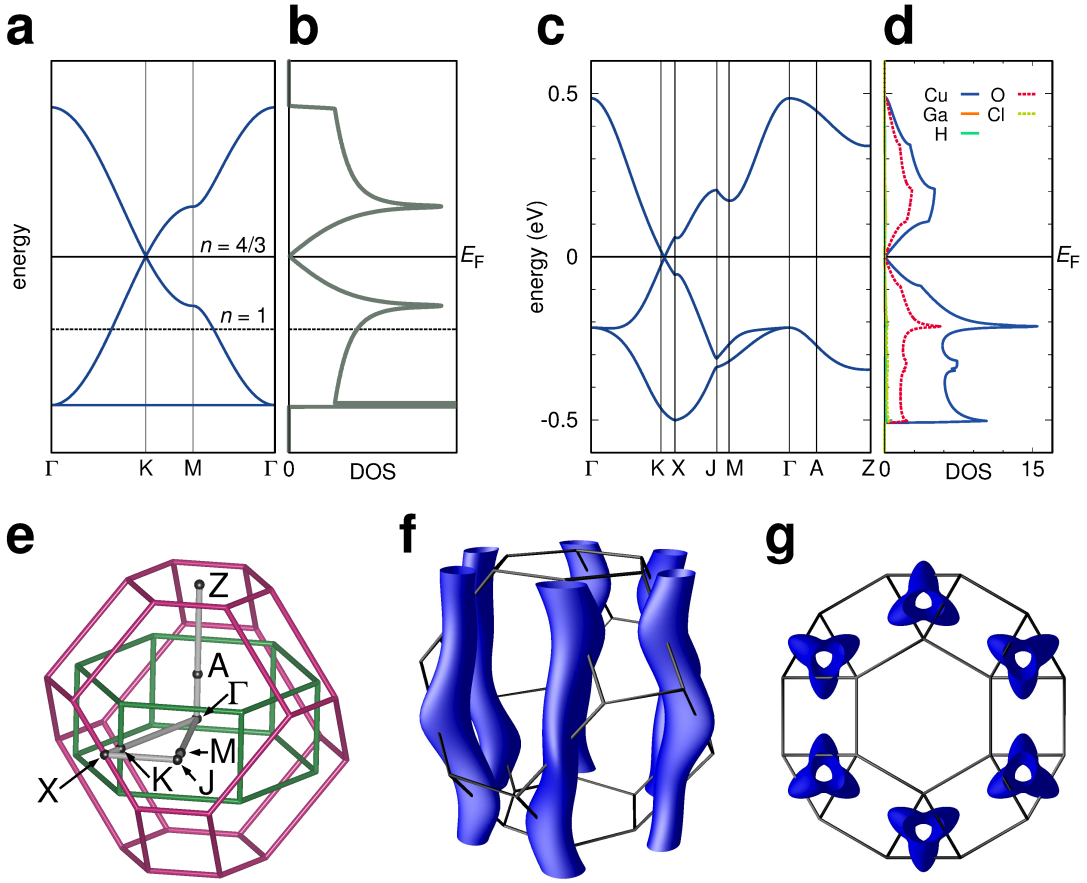

FIG. 2: Electronic structure of $GaCu_3(OH)_6Cl_2$. **a** Band structure and **b** density of states of the nearest-neighbor tight-binding model for the kagome lattice. **c**-**g** Electronic structure of Ga-substituted herbertsmithite, $GaCu_3(OH)_6Cl_2$. **c** Band structure along high symmetry points of the hexagonal setting of the $R\bar{3}m$ space group. **d** Density of states showing $GaCu_3(OH)_6Cl_2$to be a zero gap semiconductor. **e** Brillouin zones of the $R\bar{3}m$ space group in rhombohedral (purple) and hexagonal setting (green), with the path chosen in **c** (see also a view from the top in Fig. S1, Supplementary Information). **f** and **g** Fermi surfaces at an energy $E = -60$ meV. The Fermi surface plots demonstrate that the material is two-dimensional to a good approximation.

On the other hand, if all electrons are randomly distributed over all sites, each nearest neighbour bond has $(1/3)^2$=1/9 probability to have double occupancy on both sides, losing $V/9$ per bond, or $2V/9$ per site. The kinetic energy loss can be estimated as $(2/3 - 1/6) = 1/2$ of the energy of non-interacting electrons on the kagome lattice ($E_0 \approx -0.8t$ per site for $n = 4/3$),[18]. Comparing $2V/9$ and $0.4t$ we conclude that the system may develop charge ordering at $V \gtrsim 2t$. Our DFT calculations yield $t \sim 0.3$ eV, however, one may expect a renormalisation due to correlation effects; a factor of two is reasonable for Cu d electrons and we get $V_c \sim t \sim 0.3$ eV. This value is much larger than V estimated for $GaCu_3(OH)_6Cl_2$, and, therefore, it should remain a uniform metal.

Again, we subjected these qualitative arguments to a numerical test solving Eq. 1 within the DCA(RISB) for $U = 5$ eV and different V values. At a critical $V_c = 0.54$ eV, (Fig. 4 **b**,**c**) well above the estimated value of $V \approx 0.11$ eV, the system charge orders and loses its metallicity, consistent with the qualitative arguments above. Interestingly, close to and inside the insulating phase the system shows substantially increased values of the intersite terms in the quasi-particle weight (Fig. 4 **d**) as well as in the cluster orbital density matrix (Fig. 4 **e**). Inspection of the slave-boson multiplet amplitudes reveal an insulator composed of dominant coherent superpositions of the four-particle triangular-cluster states with one double-occupied site and two single-occupied sites with different spin orientation, a reflection of proximity to charge ordering at $V_c = 0.54$ eV.

Note that in our functional renormalisation group (fRG) calculations, described below, the problem of the phase instabilities is approached from the opposite limit, namely the itinerant/weak coupling limit, valid at $U \lesssim t$, appropriate for addressing the superconductivity. It is worth mentioning though, that in fRG the V_c needed to stabilise the leading charge ordering instability was also far greater than the realistic range of V.

Ferromagnetism.- We consider next the possibility of a ferromagnetic instability. It is well known that Hubbard models with very large U/t and away from half-filling show propensity to so-called Nagaoka fer-

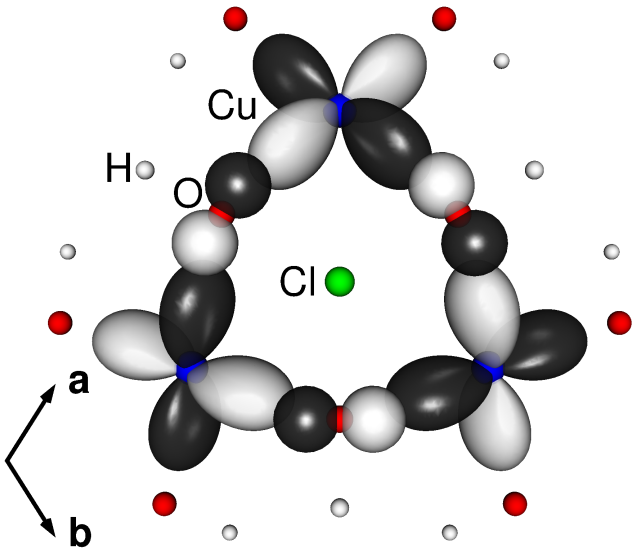

FIG. 3: Relevant tight-binding orbitals for $GaCu_3(OH)_6Cl_2$. Overlap between Cu $3d_{x^2-y^2}$ and O p orbitals in a Cu triangle. $+$ and $-$ sign of the wave function is coded with black and white, respectively.

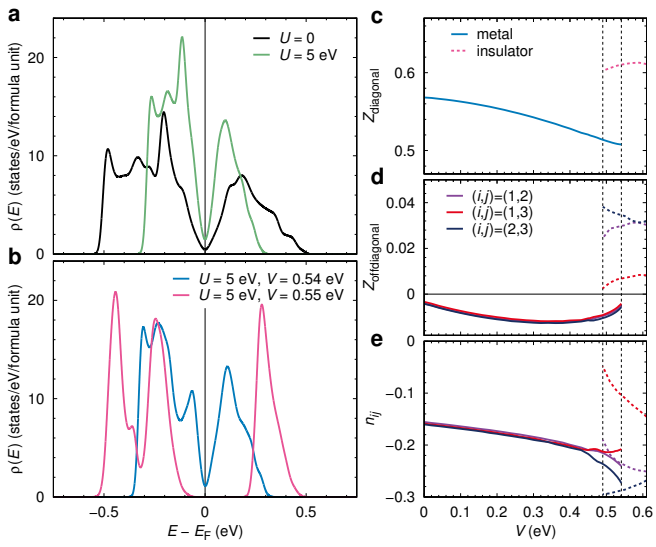

FIG. 4: DCA-like rotationally invariant slave boson results for $GaCu_3(OH)_6Cl_2$. **a**-**b** Quasi-particle (QP) spectral function for different interactions on the three-site cluster. The curves are scaled with the respective onsite QP weight$Z$. **c**-**e** cluster quantities with intersite V: onsite QP weight **c**, intersite QP weight **d**, and intersite terms of the cluster orbital density matrix **e**.

romagnetism[19]. Existing calculations[20] suggest that $GaCu_3(OH)_6Cl_2$ is far from the Nagaoka regime. However, these works did not consider states with partial spin-polarization, which are natural in a metallic system.

Let us first estimate the effective magnetic interactions at the mean-field level by comparing the superexchange $J_{ex} \sim 4t^2/U \sim 70$ meV and the ferromagnetic kinetic energy gain per bond, times the number of mobile electrons per site. $E_{KE} = E_0/3 \times 1/3 \sim 30$ meV. $E_{KE} < J_{ex}$, suggesting a spin-liquid without a long range order. However, this estimate also does not account for partial polarization, and in fact shows that the two competing interactions are of the same order of magnitude. Therefore we looked for ferromagnetism with the DCA(RISB), and found no ferromagnetism at $n = 4/3$ (Dirac metal) and $n \lesssim 4/3$ (hole-doping) for any reasonable parameters. In contrast, with electron doping ($n > 4/3$), as the superexchange is gradually suppressed, ferromagnetism becomes increasingly more favourable.

The importance of electron itineracy is particularly clear from our weak coupling fRG calculations (see the Supplementary Information). By construction, fRG shows no instabilities for zero DOS, but as we dope away from the Dirac point (either holes or electrons), we find, at sufficiently large U, a ferromagnetic instability. It should be noted that fRG depends on resummation of all parquet diagrams, an approximation not rigorously justified when U exceeds the band width. As we do not see clean divergent RG flow for the ferromagnetic channel, we cannot distinguish ferromagnetic fluctuations from a partially-polarised ferromagnet. From the combined view of different methodolgies, however, we can ascertain that the system is very close to a ferromagnetic instability; whether it is realized in $GaCu_3(OH)_6Cl_2$, we cannot be sure. But, importantly, strong ferromagnetic fluctuations are essential for unconventional superconductivity, discussed in the next section.

Superconductivity.- Finally, we investigate the possibility of superconductivity in $GaCu_3(OH)_6Cl_2$. Obviously, when the Fermi level is exactly at the Dirac point the effective DOS (averaged over the cutoff energy) is small, of the order of $J_{ex}v_F$, where the cutoff is set at the exchange energy; v_F is the Dirac velocity[21]. However if the Ga substitution is incomplete and the Fermi surfaces form narrow cylinders (Fig. 2 **f**,**g**) one expects sizeable coupling with spin excitations. This can be qualitatively estimated in the simple model of Fig. 2 **a** as follows: The pairing interaction can be written, roughly, as $t^2S(q,\omega)$, where $S(q,\omega)$ is the Fourier-transform of the spin-spin correlator $\langle S_iS_j\rangle$. Assuming that only the nearest spins are correlated (antiferromagnetically), we get three branches, one corresponding to an uncorrelated spin liquid, $S(q,\omega) = 0$, and two dispersive ones. As discussed in Ref. 22, this corresponds to three magnon modes, one dispersionless and two acoustic; the corresponding pairing interaction is strong at $q \sim 0$ and weakens for larger q values, and is repulsive for singlet and attractive for triplet pairing. Note that possible ferromagnetic fluctuations, not included in this simplistic picture, are $also$ peaked at $q \sim 0$ and thus the arguments above apply to them, too.

Now we observe that in a hexagonal Brillouin zone the 6 K-points related by the rotational symmetry (Supplementary Information, Fig. S1) can be separated into two subsets, K and K', such that all points of a given

subset are also connected by translational symmetry. Given that the superconducting order parameter has to honor translational symmetry (but not necessarily rotational one), we see that as we go around the Brillouin zone the phase factors between the consecutive pockets (neglecting intrapocket variations) vary as $\phi, \phi', \phi, \phi', \phi, \phi'$, corresponding to an $L = 3$ (f-wave) harmonic. Indeed there exists a state[23], often labelled B_{1u}, with the order parameter transforming as $\hat{\mathbf{z}}x(x^2 - 3y^2)$, so that $\phi = -\phi'$. In this case the intrapocket ($e.g.$, small q) interaction is attractive and pairing, while the interpocket one is repulsive and pairbreaking. However, the interpocket interaction is suppressed (assuming an acoustic spectrum) as $(k_F/G)^2$, with the distance $G = K - K'$. One can estimate the BCS T_c=$\omega \exp(-1/\lambda)$, where $\omega \sim Jk_F a$ (Ref. 22, Eq. 2.23), and $\lambda \sim t^2 N(E_F)/\omega \sim t/J$. We see that (i) the coupling constant is roughly independent of doping, (ii) the prefactor changes approximately as a square root of doping and (iii) one can expect a sizeable T_c for $k_F \lesssim G/2$ (the maximum possible value before changing the topology). For $\lambda \sim 1$, which seems to be a conservative estimate, and $k_F \sim G/4$, we get $T_c \sim 0.07J \sim 30$ K for $J \sim 40$ meV. Note that in this regime dependence on λ is close to linear. Taking $\lambda \sim 2$ raises the estimate for T_c to 60 K. Of course, all these estimates are order of magnitude at best, therefore we turn again to a quantitative treatment in terms of multi-sublattice fRG[24]. Note that superconductivity is an itinerant effect, and the inherent fRG assumption of weak coupling should be acceptable.

Around $n = 4/3$ and constraining ourselves to the superconducting channel, which, from a Kohn-Luttinger perspective, would become the leading channel for sufficiently weak interactions, we find a clear preference for nodeless f-wave superconductivity, as anticipated from the qualitative argument above. The calculated gaps, while changing sign between the pockets, remain uniform inside each pocket (see Supplementary Information, Fig. S3). It is worth noting that the disorder introduced by Zn doping, while weak, might even, counterintuitively, support superconductivity in this limit[25]. Finally, a subtlety could arise for significant V: In order to avoid onsite *and* nearest neighbour repulsion, this could drive a transition from a nodeless B_{1u} f-wave to nodal B_{2u} f-wave[26], but for realistic values of V this is highly unlikely.

Conclusions.- This work opens many interesting avenues toward novel physics in electron-doped herbertsmithite compounds. Bridging between an RVB scenario of frustrated magnetism for $x = 0$ and a correlated Dirac metal at $x = 1$, $Zn_{1-x}Ga_xCu_3(OH)_6Cl_2$ promises to exhibit a plethora of unconventional electronic phases as a function of doping, temperature, and disorder. Even if a solid solution $0 < x < 1$ (which would be an ultimate bonanza of novel physics) would not be realized experimentally, pure $GaCu_3(OH)_6Cl_2$ ($x = 1$) and its slightly hole doped version ($x \lesssim 1$) should be highly interesting systems, and can still be characterized as doped RVB. According to our analysis, in this regime (close to the Dirac points) the two leading candidates for the low-temperature ground state are weak ferromagnetism and f-wave superconductivity. Further experimental and theory work shall decide who is the winner in their competition.

Acknowledgements

We acknowledge useful discussions with C. Krellner, C. Platt, G. Khalliulin, A. Chubukov and C. Piefke. I.I.M. is supported by ONR through the NRL basic research program. H.O.J., F.L. and R.V. are supported by DFG-FOR1346 and DFG-SFB/TR49 (H.O.J., R.V.). R.T. is supported by the European Research Council through the grant TOPOLECTRICS, ERC-StG-336012.

Author contributions Ab initio density functional calculations, conceptual development and analysis: I.I.M., H.O.J., R.V. DCA(RISB) calculations: F.L. DCA(CT-QMC) calculations H.L. fRG calculations: M.F, R.T. All authors participated in writing the manuscript.

[1] Shores, M. P., Nytko, E. A., Bartlett, B. M. & Nocera, D. A structurally perfect $S = 1/2$ kagome antiferromagnet. *J. Am. Chem. Soc.* **127**, 13462 (2005).

[2] Lee, P. A. An end to the drought of quantum spin liquids. *Science* **321**, 1306–1307 (2008).

[3] Mendels, P. & Bert, F. Quantum kagome antiferromagnet $ZnCu_3(OH)_6Cl_2$. *J. Phys. Soc. Jpn.* **79**, 011001 (2010).

[4] Han, T.-H. *et al.* Fractionalized excitations in the spin-liquid state of a kagome-lattice antiferromagnet. *Nature* **492**, 406 (2012).

[5] Anderson, P. W. The resonating valence bond state in La_2CuO_4 and superconductivity. *Science* **235**, 1196–1198 (1987).

[6] Kivelson, S. A., Rokhsar, D. S. & Sethna, J. P. Topology of the resonating valence-bond state: Solitons and high T_c superconductivity. *Phys. Rev. B* **35**, 8865–8868 (1987).

[7] Wen, X. G. Mean-field theory of spin-liquid states with finite energy gap and topological orders. *Phys. Rev. B* **44**, 2664–2672 (1991).

[8] Klein, D., Schmalz, T. G., García Bach, M. A., Valentí, R. & Živkovic, T. P. Resonating-valence-bond theory for the square-planar lattice. *Phys. Rev. B* **43**.

[9] Yan, S., Huse, D. A. & White, S. R. Spin-liquid ground state of the $S = 1/2$ kagome Heisenberg antiferromagnet. *Science* **332**, 1173–1176 (2011).

[10] Depenbrock, S., McCulloch, I. P. & Schollwöck, U. Nature of the spin-liquid ground state of the $S = 1/2$ Heisenberg model on the kagome lattice. *Phys. Rev. Lett.* **109**, 067201 (2012).

[11] Suttner, R., Platt, C., Reuther, J. & Thomale, R. Renormalization group analysis of competing quantum phases in the J_1-J_2 Heisenberg model on the kagome lattice. *Phys. Rev. B* **89**, 020408 (2014).

[12] Jeschke, H. O., Salvat-Pujol, F., & Valentí, R. First-principles determination of Heisenberg Hamiltonian parameters for the spin-1/2 kagome antiferromagnet

$ZnCu_3(OH)_6Cl_2$. *Phys. Rev. B* **88**, 075106 (2013).

[13] Clissold, M. E., Leverett, P., Williams, P. A., Hibbs, D. E. & Nickel, E. H. The structure of gillardite, the Ni-analogue of herbertsmithite, from Widgiemooltha, Western Australia. *Can. Mineralog.* **45**, 317 (2007).

[14] Colman, R. H., Sinclair, A. & Wills, A. S. Magnetic and crystallographic studies of Mg-herbertsmithite, γ-$Cu_3Mg(OH)_6Cl_2$ – a new $S = 1/2$ kagome magnet and candidate spin liquid. *Chem. Mater.* **23**, 1811 (2011).

[15] Scott, J. D. Crystal structure of a new mineral, söhngeite. *The American Mineralogist* **56**, 355 (1971).

[16] Li, T., Wölfle, P. & Hirschfeld, P. J. Spin-rotation-invariant slave-boson approach to the hubbard model. *Phys. Rev. B* **40**, 6817–6821 (1989).

[17] Lechermann, F., Georges, A., Kotliar, G. & Parcollet, O. Rotationally invariant slave-boson formalism and momentum dependence of the quasiparticle weight. *Phys. Rev. B* **76**, 155102 (2007).

[18] In the charge-disordered state any electron has a 2/3 probability that a given neighbouring site is single-occupied and allows hopping, while in the ordered state half of the electrons are immobile, and the mobile ones have only 1/3 of the nearest neighbours single-occupied.

[19] Nagaoka, Y. Ferromagnetism in a narrow, almost half-filled s band. *Physical Review* **147**, 392 (1966).

[20] Hanisch, T., Uhrig, G. S. & Müller-Hartmann, E. Lattice dependence of saturated ferromagnetism in the hubbard model. *Phys. Rev. B* **56**, 13960–13982 (1997).

[21] Not only the coupling constant λ is small in this case, the critical temperature $T_c \propto \exp(-1/\lambda^2)$, rather than $\exp(-1/\lambda)$.

[22] Harris, A. B., Kallin, C. & Berlinsky, A. J. Possible Néel orderings of the kagome antiferromagnet. *Phys. Rev. B* **45**, 2899–2919 (1992).

[23] Sigrist, M. & Ueda, K. Phenomenological theory of unconventional superconductivity. *Rev. Mod. Phys.* **63**, 239–311 (1991).

[24] Platt, C., Hanke, W. & Thomale, R. Functional renormalization group for multi-orbital fermi surface instabilities. *Advances in Physics* **62**, 453 (2013).

[25] Nandkishore, R., Maciejko, J., Huse, D. A. & Sondhi, S. L. Superconductivity of disordered dirac fermions. *Phys. Rev. B* **87**, 174511 (2013).

[26] Kiesel, M. L., Platt, C., Hanke, W., Abanin, D. A. & Thomale, R. Competing many-body instabilities and unconventional superconductivity in graphene. *Phys. Rev. B* **86**, 020507 (2012).

Theoretical prediction of a strongly correlated Dirac metal – Supplementary Material –

I. I. Mazin,[1] Harald O. Jeschke,[2] Frank Lechermann,[3] Hunpyo Lee,[2] Mario Fink,[4] Ronny Thomale,[4] and Roser Valentí[2]

[1]*Code 6393, Naval Research Laboratory, Washington, DC 20375, USA*
[2]*Institut für Theoretische Physik, Goethe-Universität Frankfurt, Max-von-Laue-Strasse 1, 60438 Frankfurt am Main, Germany*
[3]*I. Institut für Theoretische Physik, Universität Hamburg, D-20355 Hamburg, Germany*
[4]*Institut für Theoretische Physik I, Universität Würzburg, am Hubland, 97074 Würzburg, Germany*

(Dated: March 5, 2014)

S1. First principles calculations

For structural optimization and to probe structural stability we used the projector augmented wave method as implemented in the VASP package[1,2], with the generalised gradient approximation (GGA) functional[3]. We show in Table SII the predicted structure of $GaCu_3(OH)_6Cl_2$ which can be compared to the experimental crystal structure of herbertsmithite (Table SI). Note that the optimized $GaCu_3(OH)_6Cl_2$ structure is very close to the herbertsmithite one, indicating that the kagome structure is as natural for Ga as it is Zn.

We have also verified that this structure is dynamically stable against $q \to 0$ perturbations by veryfing that the perturbed structures relax back to the original structure.

For the calculation of the dielectric constant (see below) we used the Linear Augmented Plane Wave method as implemented in the WIEN2k package[4].

Electronic structure plots of $GaCu_3(OH)_6Cl_2$, presented in this work, as well as the tight binding parameters, were obtained using the full potential local orbital (FPLO) package[5] together with the generalized gradient approximation (GGA)[3] functional. For the density of states in Fig. 2 **d** of the main text, we use a very dense $100 \times 100 \times 100$ k mesh. To obtain a tight binding representation of the Cu $3d_{x^2-y^2}$ bands near the Fermi level, we project the (Kohn-Sham) Bloch states onto localized orbitals using projective Wannier functions within the FPLO basis as described in Ref. 6.

Finally, in Fig. S1 we provide an additional view of the Brillouin zone of $GaCu_3(OH)_6Cl_2$.

TABLE SI: Experimental structure of herbertsmithite[7]. Space group $R\bar{3}m$, $a = 6.8342$ Å, $c = 14.0320$ Å, $\alpha = \beta = 90°$, $\gamma = 120°$.

type	x	y	z
Zn	0	0	0
Cu	1/3	1/6	1/6
O	0.1265	0.2529	0.1050
H	0.192	0.384	0.084
Cl	0	0	0.30521

TABLE SII: Predicted structure of $GaCu_3(OH)_6Cl_2$. Space group $R\bar{3}m$, $a = 6.97794$ Å, $c = 13.45890$ Å, $\alpha = \beta = 90°$, $\gamma = 120°$.

type	x	y	z
Ga	0	0	0
Cu	1/3	1/6	1/6
O	0.12441	0.24882	0.09852
H	0.19846	0.39692	0.06555
Cl	0	0	0.31342

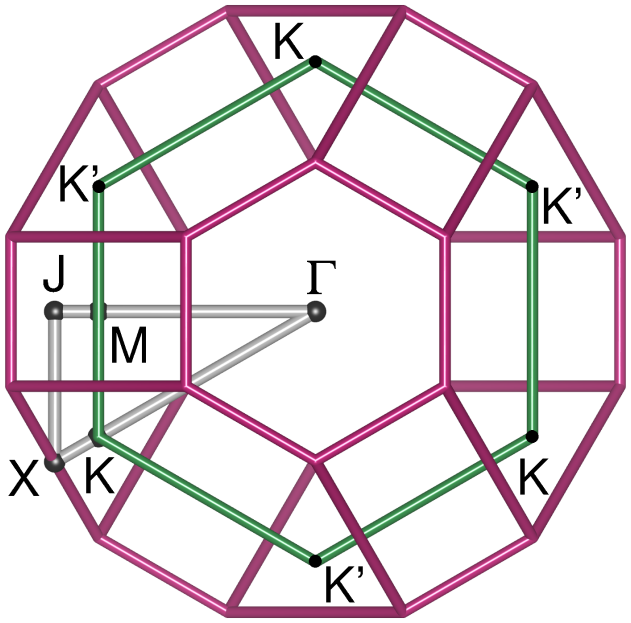

FIG. S1: Brillouin zone of $GaCu_3(OH)_6Cl_2$ viewed along the k_z direction. The Brillouin zone of the $R\bar{3}m$ space group is shown in rhombohedral (purple) and hexagonal setting (green). The path path chosen in Fig. 2 **c** of the main text is indicated in gray.

S2. Determination of U and V for $GaCu_3(OH)_6Cl_2$

The Hubbard repulsion U for copper is large, of the order of 5-7 eV. This value was obtained by using the method proposed in Ref. 8. Estimating the intersite Coulomb repulsion V is more involved. We use here the Thomas-Fermi theory for semiconductors as formulated by Resta[9] where the screened potential $V(r)$ of a point charge e is given by:

$$V(r) = \frac{e^2}{r}\frac{\sinh\kappa(R-r)}{\sinh\kappa R} + \frac{Ze^2}{\varepsilon_0 R}, \qquad (1)$$

ε_0 is the static dielectric constant, κ is the Thomas-Fermi vector defined as $\kappa^2 = 4(3\rho/\pi)^{1/3}$, and the screening parameter R is defined through the relation

$$\sinh\kappa R/\kappa R = \varepsilon_0. \qquad (2)$$

This relation is valid when $r \lesssim R$. For the total density of the valence electrons we can take $(4/3)/\Omega$, where Ω is the unit cell volume, 200 Å^3. Note that this way we totally neglect screening by other electrons but Cu $d_{x^2-y^2}$, but they probably contribute little. We calculated ε_0 and obtained $\varepsilon_{xx0} = 80$ (screening along z is much smaller, about 2.5. For simplicity we will use simply the in-plane dielectric constant), r here is the Cu-Cu distance, 3.4 Å.

Solving for R, we verify that $R = 11.2\mathring{A} \gg r$. Substituting these values into Eq. 1 we find $V(r) = 0.11$ eV[10]. For the next neighbours, $d_2 = d_1\sqrt{3}$, $V_2 = 0.03 \ll V$.

S3. DCA(CT-QMC) details

In order to account for quantum as well as short-range spatial fluctuations beyond static mean-field theory, we employ the dynamical cluster approximation (DCA) with $N_c = 3$ sites in combination with an interaction-expansion continuous-time quantum Monte Carlo approach as an exact impurity solver[11]. Fig. S2 **a** displays the density of states (DOS) for $U = 0$ to $U = 4$ eV for $T = 1/80$ with finite doping of $n = 4/3$ in the paramagnetic regime. We observe a band-narrowing but the key low energy features, especially the absence of a gap with very low DOS at E_F reflecting the Dirac points, remain.

In order to see more clearly whether the pseudogap-like structure at E_F is related to the Dirac cone, we show the imaginary parts of the self-energy as a function of Matsubara frequency for $U = 1$ eV to $U = 4$ eV for $T = 1/80$ with finite doping of $n = 4/3$ in Fig. S2 **b**. The behaviour of the imaginary part of the selfenergy follows Landau Fermi-liquid theory, where $\mathrm{Im}\,\Sigma(i\omega_n)$ approaches zero as $\omega_n \to 0$. This behaviour is also observed in DCA calculations for the honeycomb lattice, where the Dirac cones are also present[12]. This indicates that the onsite interaction alone is insufficient to drive the system insulating at the filling $n = 4/3$, in agreement with the results from the DCA(RISB) approach.

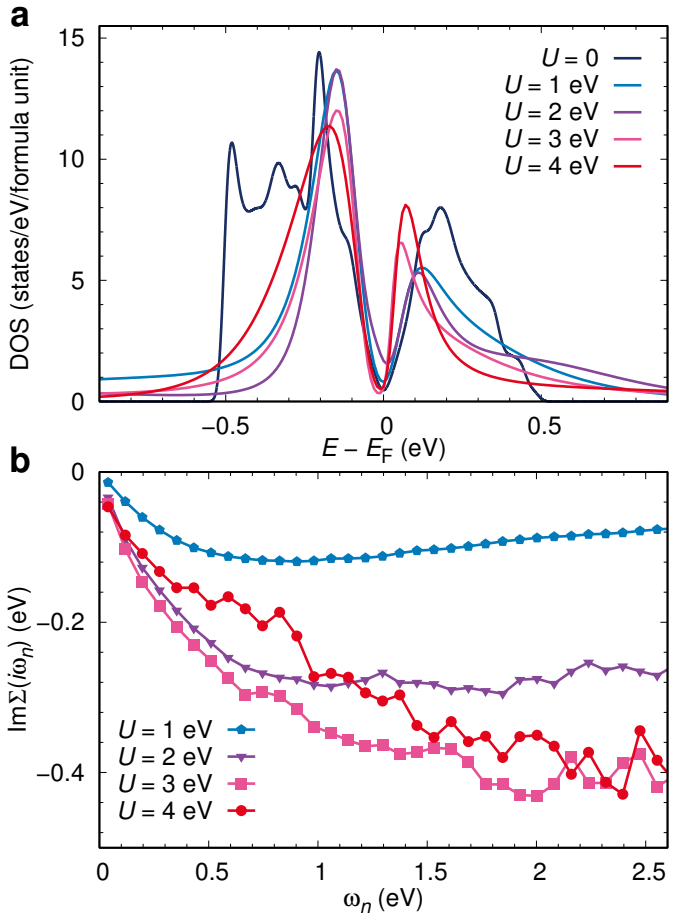

FIG. S2: **a** Density of states (DOS) at $T = 1/80$ eV with finite doping $n = 4/3$ in the paramagnetic regime. The DOS is obtained from 3-site DCA in combination with a CT-QMC impurity solver. The analytic continuation is performed using a maximum entropy method. **b** Imaginary part of onsite self-energy as a function of Matsubara frequency at $T = 1/80$ eV with the filling $n = 4/3$ in the paramagnetic regime.

S4. DCA(RISB) details

First, we applied DCA to the rotationally invariant slave-boson (RISB) formalism[13,14] in the saddle-point approximation. The kagome lattice calls for the minimal cluster of three sites, which was thus used for the calculations. Within the RISB scheme the electron's quasiparticle character (fermionic $f_{\nu\sigma}$) and its high-energy excitations (taken into account by the set of slave bosons $\{\phi\}$) are decomposed on the operator level through $\underline{c}_{\nu\sigma}$=$\hat{R}[\{\phi\}]^{\sigma\sigma'}_{\nu\nu'} f_{\nu'\sigma'}$, where ν is a generic orbital/site index and σ=$\uparrow,\downarrow$. The electronic self-energy $\Sigma(\omega)$ at the saddle-point is local and incorporates terms linear in frequency ω, as well as static renormalisation $\mathbf{\Sigma}^{\mathrm{stat}}$, i.e., $\mathbf{\Sigma}(\omega)$=$(1-\mathbf{Z}^{-1})\omega + \mathbf{\Sigma}^{\mathrm{stat}}$, whereby $\mathbf{Z}$ is the usual quasiparticle weight matrix. For more details see Ref. 14. Note that the similarly formulated single-site approach is very similar to the multi-orbital Gutzwiller technique[15].

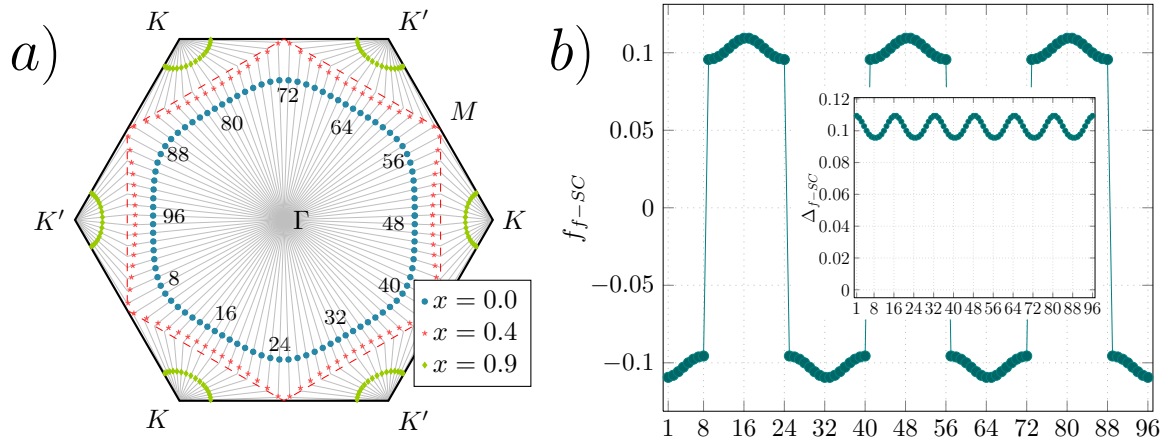

FIG. S3: a) Model Fermi surfaces interpolating from Zn-type to Ga-type filling. The Lifshitz transition happens from one contingent pocket centred around Γ to two pockets centred around K and K'. The 96-patch discretisation scheme for the FRG interaction vertex is indicated. b) Characteristic scenario at electron-doped Ga-herbertsmithite ($x = 1$): f-wave is the dominant superconducting instability with only small frustration in the Cooper channel. The superconducting form factor is depicted along the patches of a). Due to the small pockets and the nodes located along $\Gamma - M$, the SC gap looks rather homogeneous and changes sign as dictated by the B_{1u} irreducible lattice representation (inset: physical SC gap).

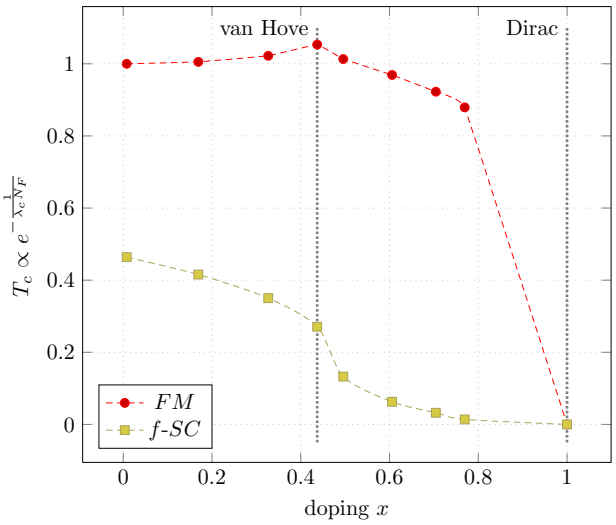

FIG. S4: Critical scale $\Lambda_c \propto T_c$ for the ferromagnetic fluctuations and f-wave superconducting instability (reference scale chosen to be the ferromagnetic scale at half filling). The critical scales are maximal around van Hove filling at the Lifshitz transition and strongly decrease as the Fermi density of states decreases towards Dirac point filling.

S5. FRG Details

We employ multi-sublattice functional RG[16] to investigate the superconducting instability for a herbertsmithite Fermiology interpolating from the Zn limit at half filling to the hole-doped Ga limit. We employ the effective two-dimensional band structure obtained from our ab initio calculations. Certainly, we cannot precisely identify at this stage for which range $x < x_c$ the Mott state persists in the compound. Instead, for our RG calculations, we assume a metallic normal state as a working hypothesis and investigate the superconducting instabilities arising for different dopings. Fig. S3a shows the Fermiology assumed for different fillings from $x = 0$ to $x = 1$. The functional RG necessitates the discretisation of the Fermi surface into patches as depicted. There is a Lifshitz transition between a single pocket centred around Γ and two pockets centred around K and K', respectively, which shrink towards points as we approach the Dirac point filling. There, the van Hove filling has been subject of intense study as the enlarged density of states at the Fermi level might propagate enhanced critical scales of unconventional Fermi surface instabilities[17,18]. However, as a major difference to e.g. a similar Fermiology on the honeycomb lattice, it should also be noted that the sublattice interference mechanism on the kagome lattice[19] significantly contributes to suppressing density wave instability with nested finite momentum transfer, providing a further bias for ferromagnetic fluctuations to dominate at higher energies.

[1] Kresse, G. & Hafner, J. *Ab initio* molecular dynamics for liquid metals. *Phys. Rev. B* **47**, 558–561 (1993).

[2] Kresse, G. & Furthmüller, J. Efficiency of ab-initio total energy calculations for metals and semiconductors using a

plane-wave basis set. *Comput. Mat. Sci.* **6**, 15 (1996).

[3] Perdew, J. P., Burke, K. & Ernzerhof, M. Generalized gradient approximation made simple. *Phys. Rev. Lett.* **77**, 3865–3868 (1996).

[4] Blaha, P., Schwarz, K., Madsen, G. K. H., Kvasnicka, D. & Luitz, J. *WIEN2k, An Augmented Plane Wave + Local Orbitals Program for Calculating Crystal Properties* (Techn. Universität Wien, Austria, 2001).

[5] Koepernik, K. & Eschrig, H. Full-potential nonorthogonal local-orbital minimum-basis band-structure scheme. *Phys. Rev. B* **59**, 1743–1757 (1999).

[6] Eschrig, H. & Koepernik, K. Tight-binding models for the iron-based superconductors. *Phys. Rev. B* **80**, 104503 (2009).

[7] Shores, M. P., Nytko, E. A., Bartlett, B. M. & Nocera, D. A structurally perfect $S = 1/2$ kagome antiferromagnet. *J. Am. Chem. Soc.* **127**, 13462 (2005).

[8] Petukhov, A. G., Mazin, I. I., Chioncel, L. & Lichtenstein, A. I. Correlated metals and the LDA+U method. *Phys. Rev. B* **67**, 153106 (2003).

[9] Resta, R. Thomas-fermi dielectric screening in semiconductors. *Phys. Rev. B* **16**, 2717–2722 (1977).

[10] Had we taken the average over the three direction $\varepsilon_0 = (80^2 2.5)^{1/3} = 25$, we would have $R = 9$, and $V(1)$ essentially unchanged, 0.12 eV.

[11] Rubtsov, A. N., Savkin, V. V. & Lichtenstein, A. I. Continuous-time quantum monte carlo method for fermions. *Phys. Rev. B* **72**, 035122 (2005).

[12] Liebsch, A. & Wu, W. Coulomb correlations in the honeycomb lattice: Role of translation symmetry. *Phys. Rev. B* **87**, 205127 (2013).

[13] Li, T., Wölfle, P. & Hirschfeld, P. J. Spin-rotation-invariant slave-boson approach to the Hubbard model. *Phys. Rev. B* **40**, 6817–6821 (1989).

[14] Lechermann, F., Georges, A., Kotliar, G. & Parcollet, O. Rotationally invariant slave-boson formalism and momentum dependence of the quasiparticle weight. *Phys. Rev. B* **76**, 155102 (2007).

[15] Bünemann, J., Weber, W. & Gebhard, F. Multiband gutzwiller wave functions for general on-site interactions. *Phys. Rev. B* **57**, 6896–6916 (1998).

[16] Platt, C., Hanke, W. & Thomale, R. Functional renormalization group for multi-orbital fermi surface instabilities. *Advances in Physics* **62**, 453 (2013).

[17] Kiesel, M. L., Platt, C. & Thomale, R. Unconventional fermi surface instabilities in the kagome Hubbard model. *Phys. Rev. Lett.* **110**, 126405 (2013).

[18] Wang, W.-S., Li, Z.-Z., Xiang, Y.-Y. & Wang, Q.-H. Competing electronic orders on kagome lattices at van Hove filling. *Phys. Rev. B* **87**, 115135 (2013).

[19] Kiesel, M. L. & Thomale, R. Sublattice interference in the kagome Hubbard model. *Phys. Rev. B* **86**, 121105 (2012).